

Optothermal Trapping of Fluorescent Nanodiamonds using a Drop-casted Gold Nanoparticle

Ashutosh Shukla,[†] Sunny Tiwari,[†] Ayan Majumder,[‡] Kasturi Saha,[‡] and
G.V.Pavan Kumar^{*,†}

[†] *Department of Physics, Indian Institute of Science Education and Research, Pune -
411008, India*

[‡] *Department of Electrical Engineering, Indian Institute of Technology, Bombay - India*

E-mail: pavan@iiserpune.ac.in

Abstract

Deterministic optical manipulation of fluorescent nanodiamonds (FNDs) in a fluid environment has emerged as an experimental challenge in multimodal biological imaging. The design and development of nano-optical trapping strategies to serve this purpose is an important task. In this letter, we show how a drop-casted gold nanoparticle (Au np) can facilitate optothermal potential to trap individual entities of FNDs using a low power density illumination (532nm laser, $0.1 \text{ mW}/\mu\text{m}^2$). We utilize the same trapping excitation source to capture the spectral signatures of single FNDs and track their position. Furthermore, by tracking the dynamics of FND, we measure the trapping stiffness as a function of laser power and surfactant concentration and emphasize their relevance as vital parameters for nano-manipulation. Our trapping configuration combines the thermoplasmonic fields generated by individual gold nanoparticles and the optothermoelectric effect facilitated by surfactants to realize a nano-optical trap down

to a single FND 120 nm in size. We envisage that our drop-casting platform can be extrapolated to perform targeted, low-power trapping, manipulation, and multimodal imaging of FNDs inside biological systems such as cells.

Keywords: Optothermal trapping, Nanodiamond, nanotweezer, optothermoelectric tweezer

Fluorescent nanodiamonds (FNDs) have emerged as a new class of imaging nanoprobe that can be adapted to various environments, including biological cells.^{1,2} The emission in FNDs is mainly due to nitrogen vacancies (NV) arrested in the diamond lattice, and they have been extensively characterized using optical spectroscopy.³ These robust nanostructures are found to be useful for multimodal spectral imaging and are extremely sensitive to perturbations in local environments.⁴ As a result, FNDs have been utilized for localized temperature nano-imaging inside a cell¹ and to extract nanoscale magnetic fields.⁵

In recent times, the FNDs have been studied in the context of optical trapping and manipulation.⁶⁻¹¹ Precise control of FNDs in solutions could increase their applicability in single spin imaging¹² and optically detected magnetic imaging.^{5,9} However, in the context of optical trapping and spectroscopy of FNDs, a majority of studies so far⁷⁻⁹ have used two laser beams, one for trapping (generally at 1064nm) and another for spectroscopy (mostly at 532nm). Although useful, this design of using separate laser beams for trapping and spectroscopy can lead to constraints due to charge state perturbations when an IR excitation is involved^{9,13} and may not be conducive in sensitive environments such as a living cell, where exposure to high-power density lasers can potentially lead to denaturing of biomolecules and damage of the cell. This clearly creates an imperative to design and develop nano-optical and optothermophoretic trapping methods¹⁴⁻²⁸ in which a single low-power laser can facilitate the capability of trapping and spectroscopic probing and imaging.²⁹ Recently, we have shown³⁰ that a drop-casted single gold nanoparticle can drive thermoplasmonic fields, facilitating the trapping of single metallic nanostructures and creating a large assembly at a very low power density ($0.01 \text{ mW}/\mu\text{m}^2$). This low power density trapping ability was facilitated by the presence of a surfactant, which creates optothermoelectric fields³¹ via ionic currents, and

enhances the attraction between the object to be trapped and the anchored gold nanoparticle (Au np). It is important to note that an anchor particle-based optothermal trapping platform^{16,17} can be used in various fluid systems, and trapping can be achieved on desired substrates. In essence, our trapping method is a nanoparticle version of optothermoelectric nano-tweezers.³¹⁻³⁴ In this study, we push the applicability of our single nanoparticle-driven thermoplasmonic trap to manipulate a single FND at a low power density of laser, which facilitates a complementary method to attract FNDs towards a plasmonic nanoparticle. We systematically studied the effect of trapping laser power and CTAC concentration in the mixture and used finite element method-based numerical calculations to compare optical and optothermoelectric force contributions. We also find that this trapping assembly is suitable for spectroscopic investigations.

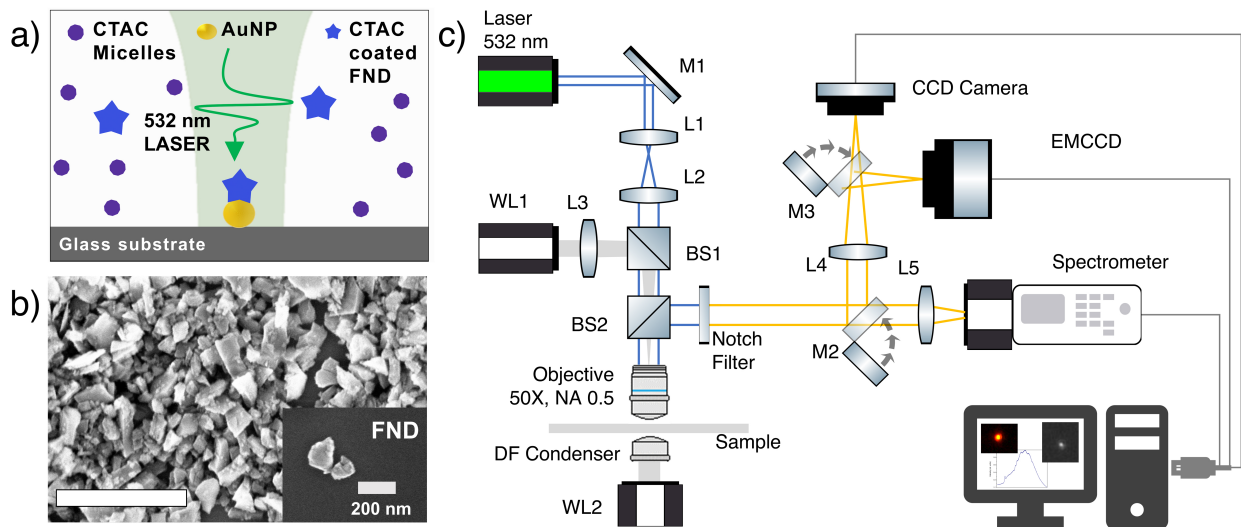


Figure 1: a) Schematic of the gold-nanoparticle driven thermoplasmonic trap. b) Scanning electron microscopy image of nanodiamonds used in this work. The scale bar on the figure is $1 \mu\text{m}$. c) Optical schematic of the trapping set-up including lenses (L), mirrors (M), beam splitters (BS), white light sources (WL), 50x objective lens of 0.5 numerical aperture, a dark field (DF) condenser of numerical aperture 1.4, a CCD camera, an electron multiplying CCD camera, and a spectrometer. This scheme integrates dark-field microscopy, optical spectroscopy, optical tracking, and fluorescent imaging.

Figure 1a shows the schematic of the gold nanoparticle-driven thermoplasmonic (GNT) trap of FNDs in a microchamber. Gold nanoparticles (Au nps) dispersed in ethanol were

drop-casted on a glass substrate, and the solvent was evaporated. A dilute solution of FNDs (Figure 1b) and surfactant (CTAC) is added to the drop-casted layer, and the chamber is sealed with an adhesive spacer and another glass coverslip. The chamber is placed on the stage of our custom-built optical trapping microscope, whose optical schematic is shown in Figure 1c. L1 and L2 are lenses used to expand the beam to overfill the back aperture of the lens. WL1 and WL2 are white light sources for top and dark-field illumination, respectively. BS1 is a beam splitter combining white light and laser light in the input path of the upright microscope. A $50\times$, 0.5 NA microscope objective focuses the incoming beam on the anchored Au np, whereas a 1.4 NA darkfield condenser focuses white light from below. The scattered light is collected by the top objective and is passed through a 532nm notch filter to remove the Rayleigh scattered light. Then the emission is sent to a CCD camera, an EMCCD, or the spectrometer using mirrors M2 and M3. Lenses L4 and L5 focus the light to form the image on cameras and spectrometer.

This upright microscope has the following capabilities: dark-field imaging to visualize the drop-casted gold nanoparticle (see supplementary information, S7); 532nm laser illumination to create a trap and excite the fluorescence in FND. The objective lens used for this purpose was a low NA (0.5) air objective lens. The focussed spot size is large compared to the spot size created by high NA objectives, which ensures that the power density delivered at the sample is low. The mechanism for the trap is discussed in supplementary information S3. The emitted fluorescence from a trapped FND was either captured by the spectrometer or directly imaged using an EM-CCD or a conventional CCD camera after rejecting the Rayleigh scattered light at 532nm. This dual camera capability was harnessed to identify single FND traps and to perform single FND fluorescence tracking.

Next, we discuss the single FND trapping in the GNT trap setup. In Figure 2a, we show the fluorescence image of a reversible trap of a single FND achieved by controlling the illumination of Au nps (see video 1 and S1 in supplementary information).

Upon illumination of a single Au np, we observed directed diffusion of FND towards the

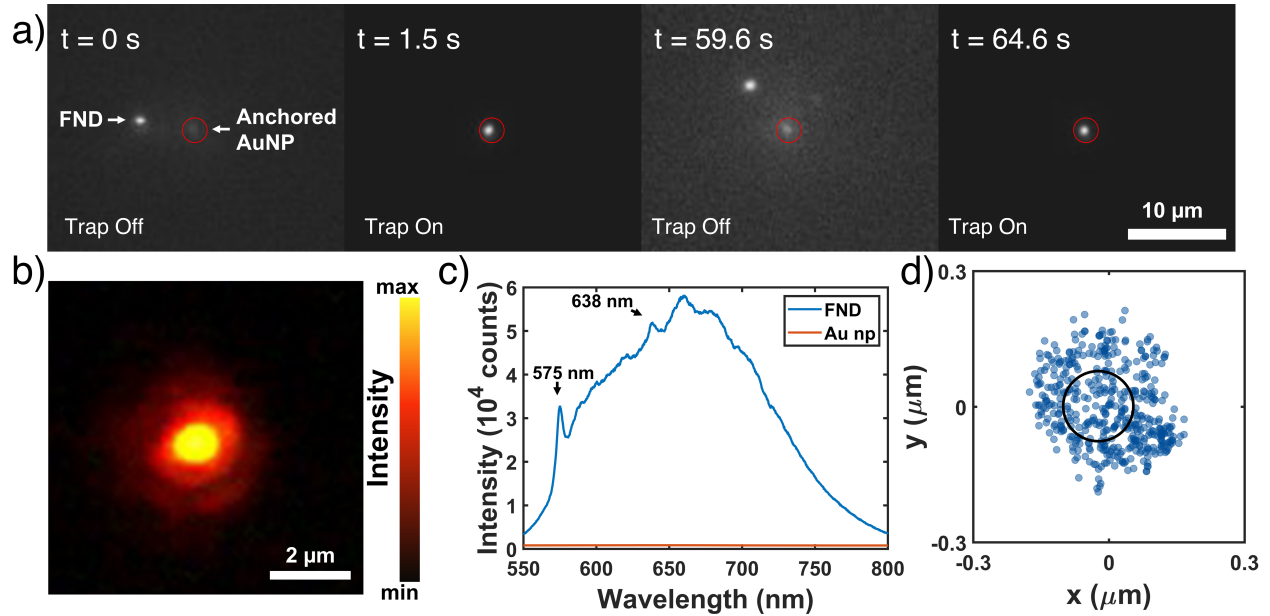


Figure 2: a) Single FND trapping using gold nanoparticle-driven thermoplasmonic (GNT) trap. The times series fluorescent images show the trap and release ability of a single FND. b) Fluorescence image of the trapped FND. The characteristic zero-phonon line at 575nm and the NV- line at 638nm are marked. c) Fluorescent spectra collected from a single FND trapped in a GNT trap. Photoluminescence from the Au np is shown in red. d) Position of a trapped FND is shown using a scatter plot. The position of Au np is shown as a black circle.

illuminated Au np. When the laser is off, the FND diffuses back to the solution. The observed switching of the FND trap was relatively quick (about 10 seconds) and could be achieved repeatedly over multiple cycles. Having trapped the FNDs, we can image it using either the fluorescence mode (see Figure 2b) or the dark field scattering mode. The same trapped FND can be spectroscopically probed, as shown in Figure 2c. In the recorded spectra, we observed the zero-phonon line at 575 nm and the NV- line at 638 nm, which indicates the charge state.⁴ These assignments fit well with the literature.^{3,4} This further indicates that the spectral features of FND are preserved in our GNT trap and can be harnessed for detailed interrogation of charge dynamics between the FND and gold nanoparticles. Such heterodimer systems can potentially read out local physical perturbation and chemical reactions in and around the illuminated Au nps. Furthermore, the fluorescence signal from trapped FND is bright enough to be used for digital tracking (see Figure 2d). We utilized this ability to study

the dynamics of FNDs in a GNT trap as a function of laser power and CTAC concentration.

A relevant aspect of measuring the displacement of FND in the trap is to find the trap stiffness as a function of parameters in the experiments. The larger the stiffness of the trap, the lesser the fluctuations. Figure 3a shows the two-dimensional position distribution (trajectories) of the trapped FNDs for four values of excitation laser powers. One can observe that the scatter in the position is more significant when the laser power is less.

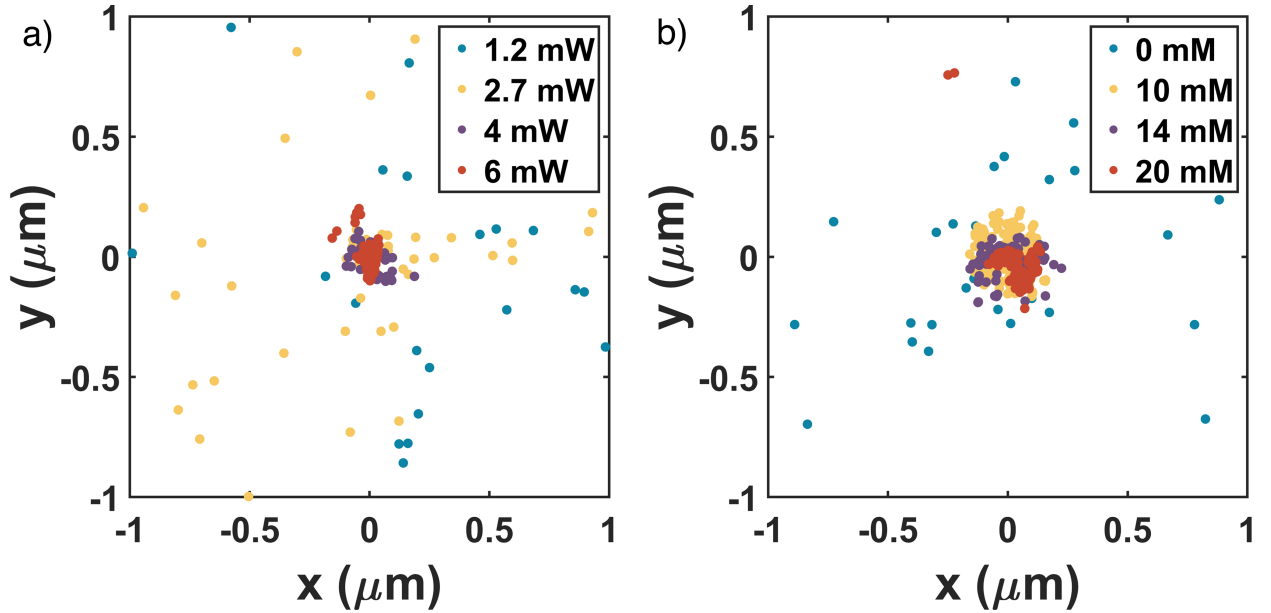


Figure 3: Position distribution of the trapped FND as a function of a) laser power and b) the CTAC surfactant concentration. As we increase the power or concentration of CTAC, the fluctuation decreases, indicating a stiffer trap.

Similarly, Figure 3b shows how CTAC concentration affects trap stiffness. We found that for increasing the CTAC concentration up to 20mM, the scatter in the trap position is reduced. The mean square displacement, σ , from the trajectories can be connected to the stiffness of the trap by the expression $\kappa = \frac{k_B T}{\sigma^2}$. From this expression, it is clear that one can obtain the trap stiffness, which tells us how tightly one can confine FNDs.

Tables I and II summarize the results for the dependence on laser power and CTAC concentration. Firstly, the stiffness of the trap uniformly increases with increasing laser power. This increased stiffness is due to the increase in temperature gradient around the drop-casted Au np. As the temperature gradient increases, so does the thermoelectric force

Table 1: Variation of trap stiffness (k_x and k_y) along x and y directions with laser power for fixed CTAC concentration (10 mM).

Power (mW)	Power density ($mW/\mu m^2$)	$k_x(pN/\mu m)$	$k_y(pN/\mu m)$
1.2	0.034	0.4	0.42
2.7	0.077	1.12	0.994
4	0.114	0.59	0.755
6	0.171	3.39	3.64

Table 2: Variation of trap stiffness (k_x and k_y) along x and y directions with concentration of surfactant (CTAC) for fixed laser power (1.2 mW).

Concentration (mM)	$k_x(pN/\mu m)$	$k_y(pN/\mu m)$
0	8.8×10^{-4}	6.9×10^{-5}
10	0.4	0.42
14	3.59	6.2
20	1.4	6.8

(see Equation 1) This shows that at nominal increments of laser power (1mW to 6 mW), one can vary the stiffness of the trap and achieve the required stability without changing any other parameter in the sample. Another way to vary the trap stiffness is to change the concentration of CTAC in the solution. As we increase the CTAC concentration, we observe an increase in the stiffness of the trap (see Table 1). This is because the thermoelectric force increases with the ionic concentration in the fluid (see Equations 1 and 2), which further facilitates the attractive potential and hence a tighter trap. Furthermore, increasing CTAC beyond 20 mM worsens trap performance, as FNDs start to stick to the glass surface.

At least two relevant forces are at play to facilitate our FND trap. The first one is the radiative, optical force component of the trap¹² that results from the electromagnetic fields due to the laser illumination. The plasmons of the Au nps also influence this force. The second is the optothermoelectric force, which results from the temperature gradient and ionic movement provided by the thermoplasmonic excitation of Au np (see Equations 1 and 2). It is relevant to compare the contribution of these forces in the trapping process. To do this, we performed three-dimensional numerical simulations based on finite element methods

(using COMSOL). In there, we extracted the optical and optothermoelectric forces (see the methods for details of the simulation).

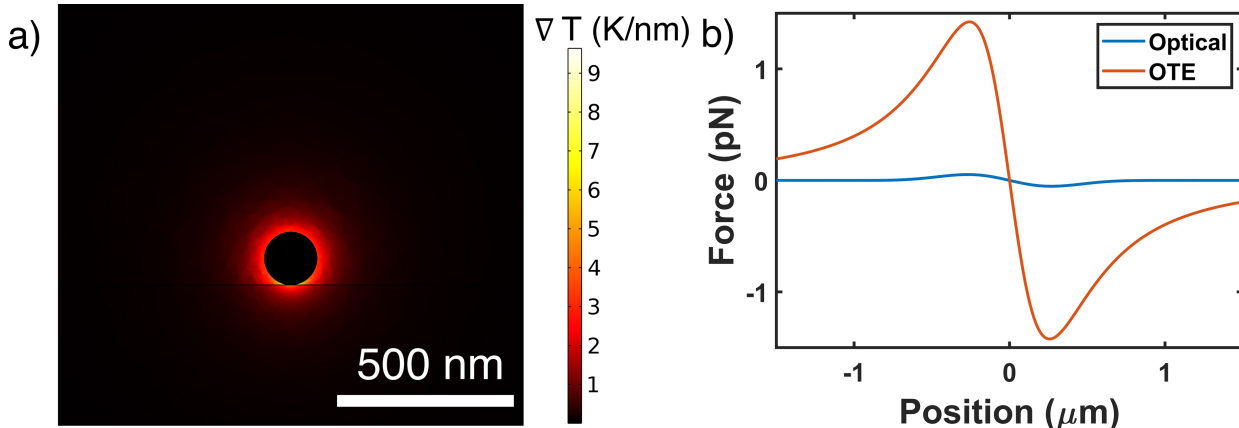


Figure 4: a) Simulated distribution of gradient of temperature in GNT trap. b) Comparison of optothermoelectric trapping (OTE) force and optical force in our geometry.

Figure 4a shows the distribution of temperature gradient facilitated by illuminating Au np at 532nm wavelength. It can be observed that the temperature gradient is sharp in the vicinity of the nanoparticle and was found to be around 5 K/nm. This sharp gradient is vital to confine the trapping region to the vicinity of the Au np, creating an opportunity to trap single nano-objects such as FND. Figure 4b compares the optothermoelectric forces (OTE) with the optical forces obtained for the same geometry. It is evident that the OTE force is dominant compared to the optical force, and therefore the resultant trapping potential is mainly facilitated by the OTE process. See supplementary information S8 for details of optical trapping experiments.

In table (III), we compare our GNT trap with other optical configurations used for FND trapping. As described, our work essentially uses a single laser excitation at nominal power to achieve trapping and spectroscopic interrogation abilities. Another specific feature of our trap is that a drop-casted gold nanoparticle is used as the origin of the trap. This implies that we can place the gold nanoparticle at the desired location on a substrate and initiate optical trapping of the FNDs. Such capability will be of immediate use in conditions such as biological cells, where one needs to place and interrogate a single FND deterministically. A

critical element in such experiments is to ensure that the spectral information is accessible, and the GNT trap discussed here may be helpful in such situations.

The various trap configurations shown in table (III) also indicate complementary capabilities; hence, our GNT trapping strategies can be harnessed, for example, in the modulated trap configuration developed by Russell et al.^{8,9}

Table 3: Comparison of our GNT trap with various configurations of FND traps in the literature.

Paper	Trapping configuration	Wavelengths (nm)	Remarks
Horowitz et al. (2012) ⁷	Conventional trap with coaxial lasers	1064, 532	The first study
Geiselmann et al. (2013) ¹²	Counter-propagating beam laser trap	1064, 532	Single spin optically manipulated, with polarization
Juan et al. (2017) ³⁵	Resonant trap with a weak perturbation	637, 532	Inspired by atomic resonant trapping
Russell et al. (2018) ⁸	Modulated trap with alternate excitation	1064, 561	Study shows IR illumination negatively affects coherence
Russell et al. (2021) ⁹	Modulated trap with alternate excitation	1064, 561	ODMR added to the modulated trap
Hong et al. (2021) ⁶	Low frequency electrothermoplasmonic tweezer	973, 532	Needs nanofabrication and electrical contacts
This work	Au np based thermoplasmonic tweezer	532	Single np as the trap center

Optical trapping of nanoparticles such as FNDs at minimum laser power has implications in multimodal imaging of biological systems such as cells and tissues. Facilitating sufficient trap stiffness to manipulate FNDs with spectroscopic imaging capability is an experimental challenge. Our work shows a pathway to achieve optothermal trapping and spectroscopy with a single excitation source (532nm) at low laser power density (around $0.1 \text{ mW}/\mu\text{m}^2$). Specifically, we have shown the relevance of laser power and surfactant concentration as

tunable parameters of trap stiffness. The realized gold nanoparticle-based traps combine optical trapping with thermophoretic and thermoelectric effects and serve as a platform for nano-manipulation in various fluid environments. By adding complementary fields such as radio frequency and weak magnetic perturbations, we envisage that our low-power trapping method can be extrapolated to optically detect magnetic resonance and single spin imaging inside a biological cell.

Materials and Methods

Sample preparation

Au nps and FNDs were purchased from Sigma Aldrich and were used as received. The reported mean diameters of Au np and FND are $150\text{nm} \pm 15\text{nm}$ and 120nm , respectively. A low concentration of Au nps was drop-casted on a glass coverslip and left to dry. FNDs were dispersed in a solution containing a specific concentration of cetyltrimethylammonium chloride (CTAC) molecules. This solution was sealed in a $120\mu\text{m}$ spacer to prevent drying and reduce convection currents.

Imaging and Tracking

The drop-casted Au np is located using the dark field scattering in the microscope. For this purpose, a high numerical aperture ($\text{NA} = 1.4$), oil immersion lens with a dark field aperture is used to condense white light from below, and a low NA (0.5), dry objective lens is used at the top to collect the light at low scattering angles. The Au np is illuminated using the same low numerical aperture objective with the laser to set up the trap. The dark field light is then turned off. The trapping force brings the FND into the vicinity of the Au np, and the FND is then imaged using its fluorescence. The collected light is sent to an EMCCD for capturing the images. The images were captured in the CCD camera at a frame rate of 35 frames per second for full frame and on the EMCCD at a frame rate of 11 fps. The position

of the FND is tracked using the TrackMate³⁶ plugin available through Fiji.³⁷ The position distribution is used to calculate the trapping strength using the equipartition method³⁸ in MATLAB.

Finite element method simulations

The temperature distribution around the nanoparticle was calculated using numerical calculations based on the finite element method using COMSOL Multiphysics (version 5.5) as a solver. The Wave optics module was coupled with the Heat transfer module to simulate the temperature increment and temperature gradient upon excitation with a light source. The simulation model consists of a 150 nm Au np placed on a glass substrate and immersed in an aqueous solution. A focused Gaussian laser source of wavelength 532 nm, which is near the absorption maxima of the Au np (see Supplementary Information S4), was used to excite the nanoparticle. This creates a temperature gradient around the Au np because of the ohmic losses. The size of the excitation spot (3.34 μm) was taken from the experimental measurements. From this thermal gradient, the thermoelectric field in our geometry was calculated as:¹⁷

$$E_T = \frac{k_B T \Delta T}{e} \left(\frac{\sum X_i c_i S_{T,i}}{\sum X_i^2 c_i} \right) \quad (1)$$

Here i denotes the ionic species, k_B is the Boltzmann constant, T is the surrounding temperature, e is the elementary charge, and c_i , and $S_{T,i}$ are the concentration and Soret diffusion coefficient of the ionic species i respectively. $X_i = \pm 1$ for positive and negative ions, respectively. The thermoelectric force, F_{TE} , is then calculated as:³⁴

$$F_{TE} = \int \sigma E_T dA \quad (2)$$

where σ is the effective surface charge density of the FND. The thermoelectric force on the FND is calculated at a height of 200 nm above the Au np. The optical force on the same particle is calculated using the Maxwell stress tensor method.³⁹ The refractive index

of Au⁴⁰ and FNDs⁴¹ were taken respectively from the literature. See supplementary info S6 for further details on the numerical calculations.

Funding

G.V.P. acknowledges financial support from the Air Force Research Laboratory grant (FA2386-18-1-4118 R&D 18IOA118) and the Swarnajayanti fellowship grant (DST/SJF/PSA-02/2017-18). A.S. acknowledges CSIR for a Junior research fellowship. K.S. acknowledges financial support from DST Inspire Faculty Fellowship DST/INSPIRE/04/2016/002284 and DST Quest Grant DST/ICPS/QuST/Theme-2/2019/Q-58.

Associated content

Supporting Information

Video showing the ability of a gold nanoparticle driven thermoplasmonic trap to trap and release a single nanodiamond. Video showing the dark-field visualisation ability along with trapping ability of the trap. Description of the videos, Transmission electron micrographs of gold nanoparticles, detailed mechanism of trapping, calculated absorption of gold nanoparticles, zeta potential of bare nanodiamonds, details of optothermoelectric force calculation, dark-field image of gold nanoparticles, comparison of optical and optothermoelectric trapping (PDF).

References

- (1) Kucsko, G.; Maurer, P. C.; Yao, N. Y.; Kubo, M.; Noh, H. J.; Lo, P. K.; Park, H.; Lukin, M. D. Nanometre-Scale Thermometry in a Living Cell. *Nature* **2013**, *500*, 54–58.

- (2) An, H.; Yin, Z.; Mitchell, C.; Semnani, A.; Hajrasouliha, A. R.; Hosseini, M. Nanodiamond Ensemble-Based Temperature Measurement in Living Cells and Its Limitations. *Meas. Sci. Technol.* **2020**, *32*, 015701.
- (3) Schirhagl, R.; Chang, K.; Loretz, M.; Degen, C. L. Nitrogen-Vacancy Centers in Diamond: Nanoscale Sensors for Physics and Biology. *Annual Review of Physical Chemistry* **2014**, *65*, 83–105.
- (4) Doherty, M. W.; Manson, N. B.; Delaney, P.; Jelezko, F.; Wrachtrup, J.; Hollenberg, L. C. L. The Nitrogen-Vacancy Colour Centre in Diamond. *Physics Reports* **2013**, *528*, 1–45.
- (5) McGuinness, L. P.; Yan, Y.; Stacey, A.; Simpson, D. A.; Hall, L. T.; Maclaurin, D.; Praver, S.; Mulvaney, P.; Wrachtrup, J.; Caruso, F.; Scholten, R. E.; Hollenberg, L. C. L. Quantum Measurement and Orientation Tracking of Fluorescent Nanodiamonds inside Living Cells. *Nature Nanotech* **2011**, *6*, 358–363.
- (6) Hong, C.; Yang, S.; Kravchenko, I. I.; Ndukaife, J. C. Electrothermoplasmonic Trapping and Dynamic Manipulation of Single Colloidal Nanodiamond. *Nano Lett.* **2021**, *21*, 4921–4927.
- (7) Horowitz, V. R.; Alemán, B. J.; Christle, D. J.; Cleland, A. N.; Awschalom, D. D. Electron Spin Resonance of Nitrogen-Vacancy Centers in Optically Trapped Nanodiamonds. *Proceedings of the National Academy of Sciences* **2012**, *109*, 13493–13497.
- (8) Russell, L. W.; Ralph, S. G.; Wittick, K.; Tetienne, J.-P.; Simpson, D. A.; Reece, P. J. Manipulating the Quantum Coherence of Optically Trapped Nanodiamonds. *ACS Photonics* **2018**, *5*, 4491–4496.
- (9) Russell, L. W.; Dossetor, E. C.; Wood, A. A.; Simpson, D. A.; Reece, P. J. Optimizing Optical Tweezers Experiments for Magnetic Resonance Sensing with Nanodiamonds. *ACS Photonics* **2021**, *8*, 1214–1221.

- (10) Perdriat, M.; Pellet-Mary, C.; Huillery, P.; Rondin, L.; Hétet, G. Spin-Mechanics with Nitrogen-Vacancy Centers and Trapped Particles. *Micromachines* **2021**, *12*, 651.
- (11) Rivière, F.; de Guillebon, T.; Raynal, D.; Schmidt, M.; Lauret, J.-S.; Roch, J.-F.; Rondin, L. Hot Brownian Motion of Optically Levitated Nanodiamonds. *ACS Photonics* **2022**, *9*, 420–425.
- (12) Geiselmann, M.; Juan, M. L.; Renger, J.; Say, J. M.; Brown, L. J.; de Abajo, F. J. G.; Koppens, F.; Quidant, R. Three-Dimensional Optical Manipulation of a Single Electron Spin. *Nature Nanotech* **2013**, *8*, 175–179.
- (13) Ji, P.; Dutt, M. V. G. Charge State Dynamics of the Nitrogen Vacancy Center in Diamond under 1064-Nm Laser Excitation. *Phys. Rev. B* **2016**, *94*, 024101.
- (14) Dienerowitz, M.; Mazilu, M.; Dholakia, K. Optical Manipulation of Nanoparticles: A Review. *JNP* **2008**, *2*, 021875.
- (15) Maragò, O. M.; Jones, P. H.; Gucciardi, P. G.; Volpe, G.; Ferrari, A. C. Optical Trapping and Manipulation of Nanostructures. *Nature Nanotech* **2013**, *8*, 807–819.
- (16) Jauffred, L.; Samadi, A.; Klingberg, H.; Bendix, P. M.; Oddershede, L. B. Plasmonic Heating of Nanostructures. *Chem. Rev.* **2019**, *119*, 8087–8130.
- (17) Chen, Z.; Li, J.; Zheng, Y. Heat-Mediated Optical Manipulation. *Chem. Rev.* **2022**, *122*, 3122–3179.
- (18) Chen, Z.; Cai, Z.; Liu, W.; Yan, Z. Optical Trapping and Manipulation for Single-Particle Spectroscopy and Microscopy. *J. Chem. Phys.* **2022**, *157*, 050901.
- (19) Spesyvtseva, S. E. S.; Dholakia, K. Trapping in a Material World. *ACS Photonics* **2016**, *3*, 719–736.
- (20) Ishihara, H. Optical Manipulation of Nanoscale Materials by Linear and Nonlinear Resonant Optical Responses. *Advances in Physics: X* **2021**, *6*, 1885991.

- (21) Lehmuskero, A.; Johansson, P.; Rubinsztein-Dunlop, H.; Tong, L.; Käll, M. Laser Trapping of Colloidal Metal Nanoparticles. *ACS Nano* **2015**, *9*, 3453–3469.
- (22) S. Urban, A.; Carretero-Palacios, S.; A. Lutich, A.; Lohmüller, T.; Feldmann, J.; Jäckel, F. Optical Trapping and Manipulation of Plasmonic Nanoparticles: Fundamentals, Applications, and Perspectives. *Nanoscale* **2014**, *6*, 4458–4474.
- (23) Joby, J. P.; Das, S.; Pinapati, P.; Rogez, B.; Baffou, G.; Tiwari, D. K.; Cherukulappurath, S. Optically-Assisted Thermophoretic Reversible Assembly of Colloidal Particles and E. Coli Using Graphene Oxide Microstructures. *Sci Rep* **2022**, *12*, 3657.
- (24) Fränzl, M.; Cichos, F. Hydrodynamic Manipulation of Nano-Objects by Optically Induced Thermo-Osmotic Flows. *Nat Commun* **2022**, *13*, 656.
- (25) Kim, J.; Martin, O. J. F. Surfactants Control Optical Trapping near a Glass Wall. *J. Phys. Chem. C* **2022**, *126*, 378–386.
- (26) Gordon, R. Future Prospects for Biomolecular Trapping with Nanostructured Metals. *ACS Photonics* **2022**, *9*, 1127–1135.
- (27) Jiang, Q.; Rogez, B.; Claude, J.-B.; Baffou, G.; Wenger, J. Quantifying the Role of the Surfactant and the Thermophoretic Force in Plasmonic Nano-optical Trapping. *Nano Lett.* **2020**, *20*, 8811–8817.
- (28) Jiang, Q.; Roy, P.; Claude, J.-B.; Wenger, J. Single Photon Source from a Nanoantenna-Trapped Single Quantum Dot. *Nano Lett.* **2021**, *21*, 7030–7036.
- (29) Patra, P. P.; Chikkaraddy, R.; Tripathi, R. P. N.; Dasgupta, A.; Kumar, G. V. P. Plasmofluidic Single-Molecule Surface-Enhanced Raman Scattering from Dynamic Assembly of Plasmonic Nanoparticles. *Nat Commun* **2014**, *5*, 4357.
- (30) Tiwari, S.; Khandelwal, U.; Sharma, V.; Kumar, G. V. P. Single Molecule Surface

- Enhanced Raman Scattering in a Single Gold Nanoparticle-Driven Thermoplasmonic Tweezer. *J. Phys. Chem. Lett.* **2021**, *12*, 11910–11918.
- (31) Lin, L.; Wang, M.; Peng, X.; Lissek, E. N.; Mao, Z.; Scarabelli, L.; Adkins, E.; Coskun, S.; Unalan, H. E.; Korgel, B. A.; Liz-Marzán, L. M.; Florin, E.-L.; Zheng, Y. Opto-Thermoelectric Nanotweezers. *Nature Photon* **2018**, *12*, 195–201.
- (32) Liu, S.; Lin, L.; Sun, H.-B. Opto-Thermophoretic Manipulation. *ACS Nano* **2021**, *15*, 5925–5943.
- (33) Ren, Y.; Chen, Q.; He, M.; Zhang, X.; Qi, H.; Yan, Y. Plasmonic Optical Tweezers for Particle Manipulation: Principles, Methods, and Applications. *ACS Nano* **2021**, *15*, 6105–6128.
- (34) Wang, X.; Yuan, Y.; Xie, X.; Zhang, Y.; Min, C.; Yuan, X. Graphene-Based Opto-Thermoelectric Tweezers. *Advanced Materials* **2022**, *34*, 2107691.
- (35) Juan, M. L.; Bradac, C.; Besga, B.; Johnsson, M.; Brennen, G.; Molina-Terriza, G.; Volz, T. Cooperatively Enhanced Dipole Forces from Artificial Atoms in Trapped Nanodiamonds. *Nature Phys* **2017**, *13*, 241–245.
- (36) Tinevez, J.-Y.; Perry, N.; Schindelin, J.; Hoopes, G. M.; Reynolds, G. D.; Laplan-tine, E.; Bednarek, S. Y.; Shorte, S. L.; Eliceiri, K. W. TrackMate: An Open and Extensible Platform for Single-Particle Tracking. *Methods* **2017**, *115*, 80–90.
- (37) Schindelin, J. et al. Fiji: An Open-Source Platform for Biological-Image Analysis. *Nat Methods* **2012**, *9*, 676–682.
- (38) Jones, P. H.; Marag-, O. M.; Volpe, G. *Optical Tweezers: Principles and Applications*; Cambridge University Press, 2015.
- (39) Jackson, J. D. *Classical Electrodynamics, 3ed*, third edition ed.; Wiley: Hoboken, NY, 2007.

- (40) Johnson, P. B.; Christy, R. W. Optical Constants of the Noble Metals. *Phys. Rev. B* **1972**, *6*, 4370–4379.
- (41) Phillip, H. R.; Taft, E. A. Kramers-Kronig Analysis of Reflectance Data for Diamond. *Phys. Rev.* **1964**, *136*, A1445–A1448.

Supporting Information

Optothermal Trapping of Fluorescent Nanodiamonds using a Drop-casted Gold Nanoparticle

Ashutosh Shukla[†], Sunny Tiwari[†], Ayan Majumder[‡], Kasturi Saha[‡], and G V Pavan Kumar^{*,†}

[†]Department of Physics, Indian Institute of Science Education and Research (IISER), Pune
411008, India

[‡]Department of Electrical Engineering, Indian Institute of Technology Bombay, India
^{*}email: pavan@iiserpune.ac.in

Contents

S1 Description of the videos	S2
S2 TEM Images of the gold particles	S3
S3 Mechanism of trapping	S4
S4 Calculated absorption spectra of Au nps	S5
S5 Zeta potential	S6
S6 Force calculation	S7
S7 Dark field image of the gold particles	S8
S8 Comparison of Optical trapping and Optothermoelectric trapping	S9

S1 Description of the videos

Clip 1

A single FND is visible at the beginning of the video, which is diffusing towards the anchor Au np. Its fluorescence intensity increases as it approaches trap center. The total intensity is scaled for better visibility. The FND gets trapped and stays in trap for about 5 seconds. The laser is then switched on and off to allow the FND to diffuse away. It is again recaptured and stays in the trap for as long as the trap is active.

Clip 2

Individual FND diffuses towards the anchored Au np, which is at the center of the screen. The FND gets trapped and the trap stays active for about 30 seconds. The laser is then switched on and off to allow the FND to diffuse away. The dark field illumination is then turned which shows multiple FNDs floating around and four drop-casted Au nps dispersed on the sample plane. The position of the Au np is checked to be at the laser center and then the trap is turned on after turning the dark-field illumination off. This is done to ensure that only illumination from FNDs is captured, which helps in accurate tracking and spectral information processing. The FND is readily trapped as shown.

The videos are recorded at 20 mM concentration of CTAC and 4 mW laser power.

S2 TEM Images of the gold particles

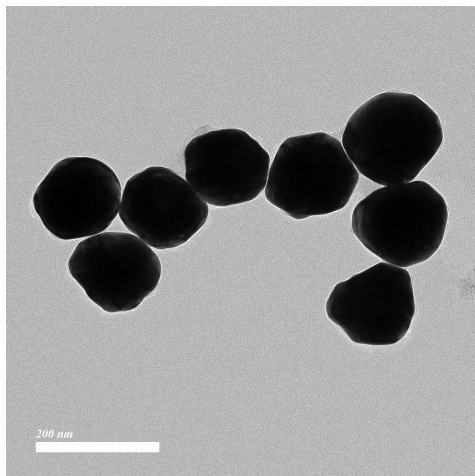


Fig. S1: Transmission electron micrograph of Gold nanoparticles. The average size of particles is 150 nm with a distribution of ± 15 nm.

S3 Mechanism of trapping

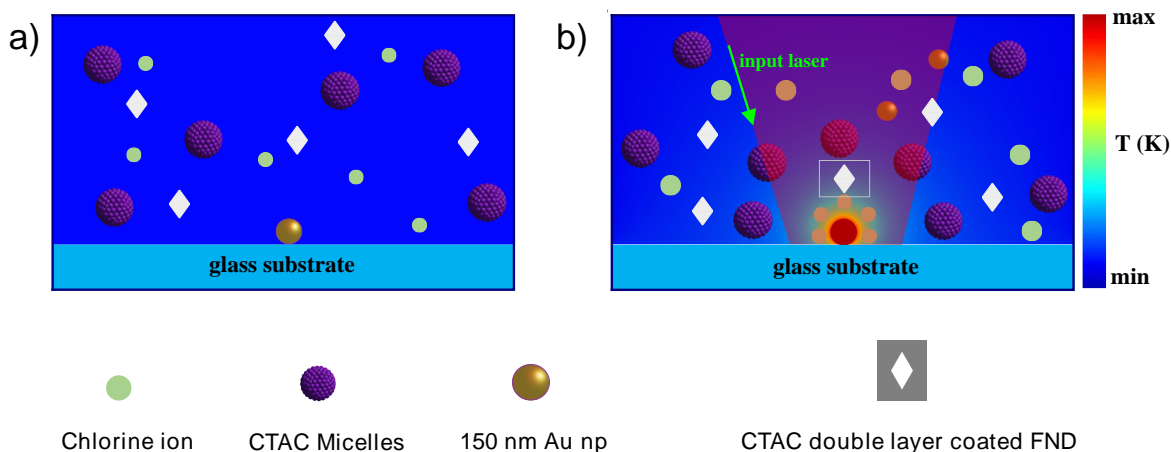


Fig. S2: Detailed mechanism of reversible trapping of FND using single nanoparticle driven thermoplasmonic trap.

The figure S2 shows the mechanism of reversible trapping. Au nps are drop-casted on glass surface and dried in a desiccator. A chamber is prepared in which the solution containing FNDs, and CTAC molecules of desired concentration is put. The chamber is then sealed using another glass slide. The CTAC molecule dissociates into Chlorine ion and the corresponding positively charged ion. The long chained positive ion coats the FNDs and the Au nps with a bilayer making them positively charged. The solution also contains micelles of the CTAC.

When the Au np is illuminated with laser, a temperature gradient is set up in the surrounding fluid. Due to difference in the Soret thermodiffusion coefficient of the positive CTAC micelles and the chlorine ions, a separation of charge occurs. The CTAC micelles, larger in size, have a higher Soret coefficient and move farther away from the heat source while the chlorine ions do not move that far away as shown in Figure S2 (b). This creates an electric field which pulls any positively charged particle towards the heat source. The trap can be turned off by turning the laser off as the charges get redistributed when the temperature gradient is removed.

S4 Calculated absorption spectra of Au nps

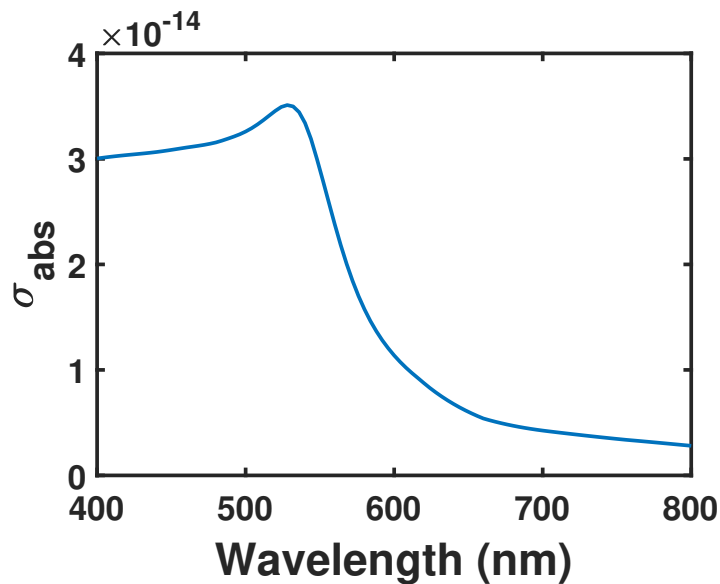


Fig. S3: Calculated absorption cross section of the drop-casted Au np.

The absorption cross section was calculated using this effective refractive index ($n_{eff} = 1.365$) to represent Au np on a glass substrate surrounded by water. This effective refractive index was calculated by matching the experimentally measured scattering cross section of the Au nps with calculated refractive index of a 150nm Au np.

The peak of this absorption cross section lies very close to 532nm. We therefore use this particular combination of particle size and laser wavelength.

S5 Zeta potential

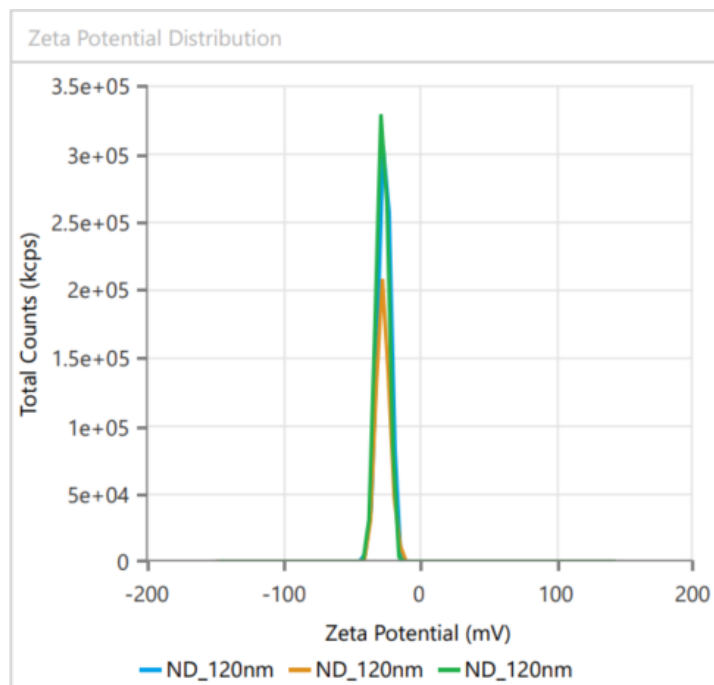


Fig. S4: Measured Zeta potential of FNDs before treating them with CTAC.

The zeta potential of the particles was measured to be -25 mV with a deviation of 4.5 mV.

S6 Force calculation

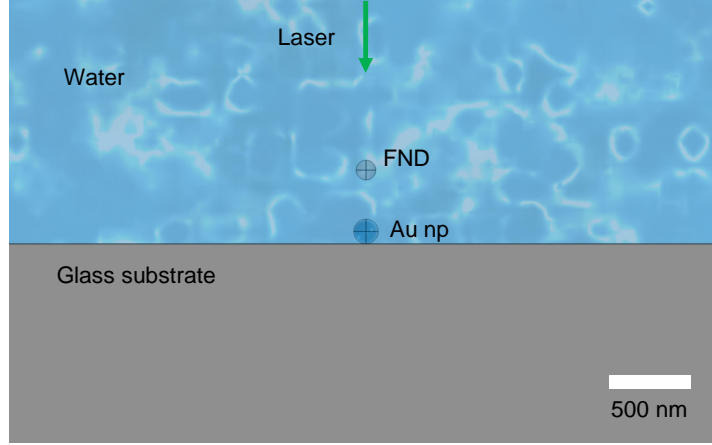


Fig. S5: Snapshot of geometry used for numerical calculation of the temperature gradient around the particle.

As mentioned in the main text, the thermoelectric force on the FND was calculated using the following equations:

$$E_T = \frac{k_B T \Delta T}{e} \left(\frac{\sum X_i c_i S_{T,i}}{\sum X_i^2 c_i} \right) \quad (1)$$

Here i denotes the ionic species, k_B is the Boltzmann constant, T is the surrounding temperature, e is the elementary charge, and c_i , and $S_{T,i}$ are the concentration and Soret diffusion coefficient of the ionic species i respectively. $X_i = \pm 1$ for positive and negative ions, respectively. The $S_{T,CTAC}$ and $S_{T,Cl}$ are taken from references [1, 2] respectively.

The thermoplasmonic thermal gradient generated by the Au np is calculated numerically using COMSOL 5.5. The geometry used is shown in Figure S5.

The thermoelectric force, F_{TE} , is then calculated as:

$$F_{TE} = \int \sigma E_T dA \quad (2)$$

where σ is the effective surface charge density of the FND. It was calculated using the Gouy-Chapman relation [3].

The force profile shown in Figure 4b is calculated by scanning the FND along x direction at a distance of 200 nm above the Au np. The optical force was calculated on the same assembly by integrating the Maxwell's stress tensor on the surface of the FND. Spherical particles were assumed and no thermal effects were included while calculating the optical force.

S7 Dark field image of the gold particles

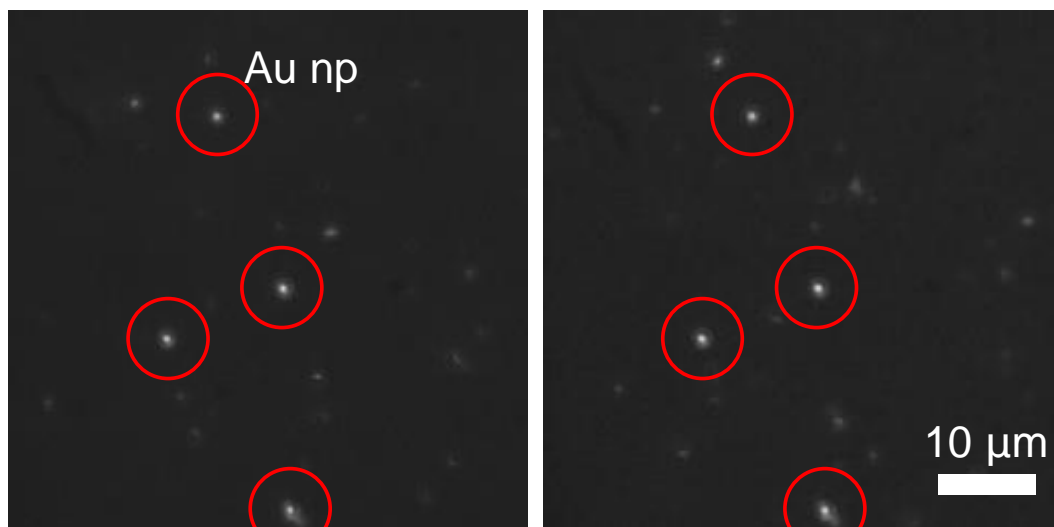


Fig. S6: Dark field image (captured in EMCCD) showing Au nps with fainter FNDs floating around. The two panels of the image show drift in position of FNDs while the anchor Au nps stay in place.

S8 Comparison of Optical trapping and Optothermoelectric trapping

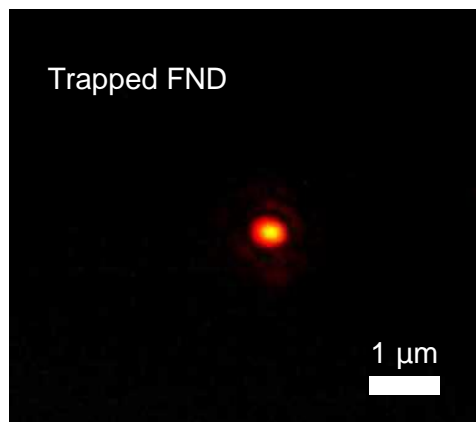


Fig. S7: Fluorescence image of optically trapped multiple FNDs.

The nanodiamonds were optically trapped in same setup using an objective lens of 0.5 numerical aperture. The trapping is done at a relatively higher concentration. Thus multiple particles come in the beam spot and are trapped. The power required to stably trap the FNDs this way in the setup exceeds 20 mW.

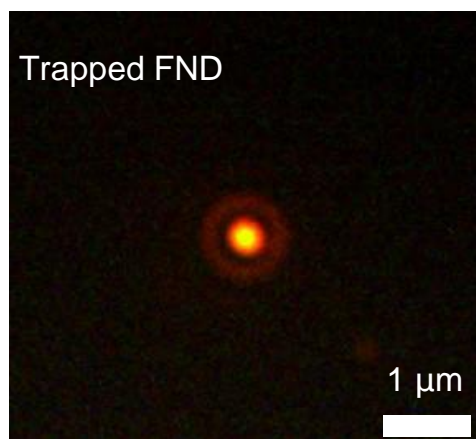


Fig. S8: Fluorescence image of single optically trapped FND using a water immersion objective lens (NA 1.2).

To maximize the trapping efficiency for optical trapping we used an objective lens with high numerical aperture to increase the gradient force. The input power required to trap the particle is more than 15 mW with this setup.

References

- [1] Daniele Vigolo, Stefano Buzzaccaro, and Roberto Piazza. Thermophoresis and thermoelectricity in surfactant solutions. *Langmuir*, 26(11):7792–7801, 2010. PMID: 20146491.
- [2] J. N. Agar, C. Y. Mou, and Jeong Long Lin. Single-ion heat of transport in electrolyte solutions: a hydrodynamic theory. *The Journal of Physical Chemistry*, 93(5):2079–2082, 1989.
- [3] Zhenpeng Ge and Yi Wang. Estimation of nanodiamond surface charge density from zeta potential and molecular dynamics simulations. *The Journal of Physical Chemistry B*, 121(15):3394–3402, 2017. PMID: 28423901.